ISIJ International, Vol. 51 (2011), No. 8, pp. 1204–1212

Binding Energy of Carbon Implanted into Hematite and *in situ* Observation of Reaction Behavior during Heating Up Experiment

Yoshiaki KASHIWAYA,[1] Tsuyoshi NAKAMITSU,[2] Hiroshi KINOSHITA[3] and Seiji MIURA[3]

1) Formerly Graduate School of Eng., Hokkaido University. Now at Kyoto University.
2) Faculty of Eng., Hokkaido University. 3) Graduate School of Eng., Hokkaido University.

(*Received on November 16, 2010; accepted on February 23, 2011*)

It is widely known that the direct contact between solid carbon and iron oxide shows quite a fast reduction rate in comparison with CO gas reduction. However, it is difficult to sustain the physical contact between solid carbon and iron oxide. Furthermore, the contact mode will be different from the production method, which will affect the reaction kinetics strongly.

In this study, different kinds of contacts between solid carbon and hematite were made to clarify the reaction mechanism. One contact mode is the deposition of the carbon layer on the hematite surface using a vacuum evaporation method. Another method is the implantation of carbon ions into hematite. Using XPS (X-ray photoelectron spectroscopy), the binding energy of Fe–O–C was measured. Heating under an argon atmosphere was carried out. Both samples showed quite different reaction behavior, though the temperature at the beginning of the reduction reaction was almost the same. From these results, it was determined that the position of carbon will change the reaction behavior drastically, because it is important how the CO gas escapes from the reaction site.

KEY WORDS: direct reduction; reaction with solid carbon; XPS; binding energy.

1. Introduction

Recently, worldwide issues such as global warming by greenhouse gases like CO_2 and the rapid jump in energy prices have attracted the interest of many people. The steel industry exhausts a large amount of CO_2 because a lot of carbon (coal) is required as a reducing agent and heat source for producing iron and steel, although Japanese steel industries are making steel with the lowest CO_2 emission in the world. However, because the absolute value of crude steel production is huge, the percentage of energy consumption is also high. It is about 15% (49.2 Mton-C) in total Japanese CO_2 exhaust and about 12% (2 380 PJ) in total Japanese energy consumption. From this point of view, energy saving and the reduction in CO_2 emissions from the steel industries are quite effective and contribute not only to Japan, but also to the world.

Ironmaking processes require much energy and consume about 70% of the energy in the entire steelmaking process. However, the blast furnace (BF) process is still the main process among the several ironmaking processes because the BF method has a high reaction and heat efficiency. There are many campaigns to increase those efficiencies, such as PCI (pulverized coal injection), recycle of BFG (blast furnace gas) and electric power generation using the top gas pressure. However, even in such highly efficient BF processes, there is some possibility to increase the efficiency from the view point of a chemical reaction, because the utilization of CO gas is about 50% and is expected to modify the efficiency theoretically.

The key to achieving this increase in efficiency is to increase the rates of the reduction reaction of iron ore and the gasification reaction of coke, respectively. Furthermore, the coupling reaction between gasification reaction and reduction reaction should be enhanced. The goal of enhancing the coupling reaction is to decrease the temperature of the reserve zone, which corresponds to a decrease in the fuel rate. Until now, the effects of the coupling reaction to decrease the fuel rate by controlling the arrangement between the iron ore and coke from a macroscopic to a microscopic level have been studied in the research group of the "Control of Reduction Equilibrium in BF through Vicinity Arrangement of Iron Ore and Carbon" held in ISIJ. We have studied this research area from the perspective of a microscopic and nanoscopic coupling reaction.

The reduction reaction of iron oxide by solid carbon occurs from the direct contact between carbon and iron oxide—a so-called solid-solid reaction. Recently, it was found that the direct reduction with solid carbon could proceed first and in a lower temperature range in comparison with CO reduction, which is dominant in the BF process.[1–4] Until now, we have studied the reaction behaviors between solid carbon and iron oxide by changing the contact conditions; for example, (i) mechanical milling of the mixture of carbon and iron oxide, (ii) the carbon layer on the hematite surface using vacuum evaporation method and so on. From another point of view, these conditions change the binding state among Fe–O–C atoms; to be specific, the initial reaction rate is strongly affected by the contact conditions because the ultimate contact mode can induce a forward

chemical reaction.

In this study, the ultimate contact between carbon and iron oxide was made by carbon ion implantation into the hematite structure. After implantation, the reaction behaviors were investigated by heating up condition under an inert atmosphere. Moreover, the binding energies among Fe, C and O atoms were examined using XPS (X-ray photoelectron spectroscopy) and the relationship between the binding energies and reaction behaviors was analyzed.

2. Experimental Procedures

2.1. Preparation of the Hematite Sample

In this experiment, a hematite pellet was prepared by the procedures shown in **Fig. 1**. The size of the pellet was 20 ϕ O.D. × 5 mm H. A reagent hematite sample of high purity (>99.0%) was weighted to about 4–5 g and pressed in a stainless mold (20 mm ϕ, I.D.) by 19.6 MPa (200 kgf/cm^2), which was increased with stepwise pressing every 4.9 MPa (50 kgf/cm^2). After reaching 19.6 MPa, the pressure was held constant for 24 h in order to minimize the stress inside the hematite pellet, to prevent the pellet from being broken during heating in the next procedure. The pellet was sintered under an air atmosphere at 1 100°C for 168 h in a muffle furnace to increase the grain size (about 20 μm). After sintering, the top surface of the pellet was polished until #1500 with dry emery polishing paper.

2.2. Hematite Samples Implanted with Carbon Ions and Carbon Layer by Vacuum Vapor Deposition

Figure 2 illustrates hematite samples contacted with two forms of carbon. Figure 2(a) shows a hematite sample with a carbon layer about 300 nm thick. The details of the experimental method have been published elsewhere.[5] Figure 2(b) illustrates carbon ion implantation into hematite. Two kinds of implantation conditions were adopted so that the concentration of ions was 1.0×10^{17} ions/cm^2 under one condition and 5.0×10^{17} ions/cm^2 under the other. The acceleration voltage for both conditions was 220 kV. The ion current densities for each condition were 1.0 μA/cm^2 and 3.0 μA/cm^2, respectively, and the time for implantation was controlled for the desired ion concentration. In this study, the former sample with a low concentration of implanted ions is referred to as "Imp-1" and the latter is referred to as "Imp-2" for convenience.

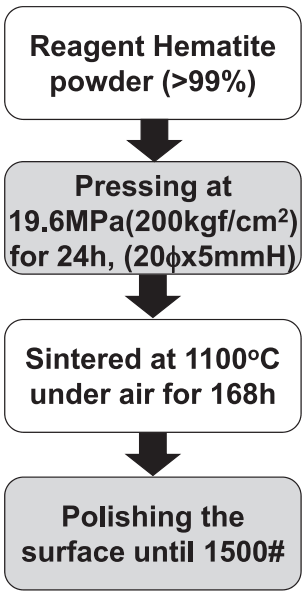

Fig. 1. Procedure of hematite sample pellet preparation.

2.3. SEM Observation and EDS Analysis

To determine the change in the sample surface before and after implantation, SEM observation was performed. In addition, the cross-section of the sample after implantation was also examined by SEM, and the line analysis of C, Fe and O from the surface to the inside was performed by EDS. Moreover, a simulation calculation to confirm the distribution of C atoms implanted in the hematite was carried out using program code SRIM2300.[6]

The XPS (JPC-9010MC) measurements were carried out on three hematite samples with carbon layer, Imp-1 and Imp-2. The binding energies of C, O and Fe as a function of the depth from the surface were measured using Al–Kα characteristic X-ray irradiation after Ar ion sputtering, in which the conditions were 3 000 eV, 20 mA and a sputtering rate of 0.648 nm/s, which was estimated for the pure hematite sample used in this study.

2.4. Heating Up Experiment

Heating up experiments were carried out using an infrared image furnace equipped with a laser microscope.[5] The behavior of the samples Imp-1 and Imp-2 were directly observed during heating under an Ar (P_{O2}<0.002 ppm) atmosphere. The samples were heated up to 1 000°C within 3 minutes (5.56 K/s), held for 30 minutes, and then quenched to room temperature in 3 minutes. The *in situ* observations were performed from heating to cooling.

Before and after the heating up experiment, SEM observations of the surface were performed to determine the differences in surface morphology.

3. Results and Discussions

3.1. SEM Observation of the Surface Before and After Carbon Implantation

Figure 3 shows an SEM image of the surface of Imp-1

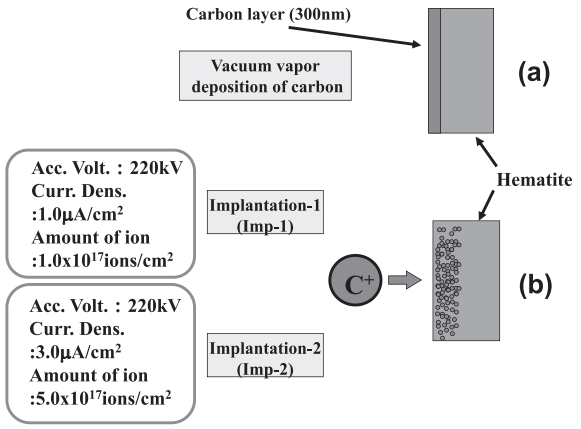

Fig. 2. Illustration of (a) carbon layer (300 nm) by vacuum vapor deposition and (b) carbon ion implantation into hematite (Imp-1 and Imp-2).

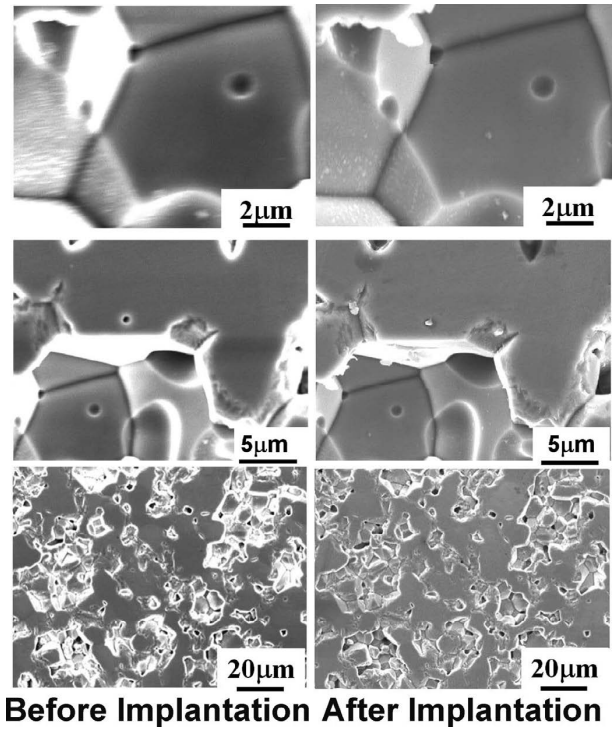

Fig. 3. Result of SEM observation of hematite surface before and after implantation (Imp-1).

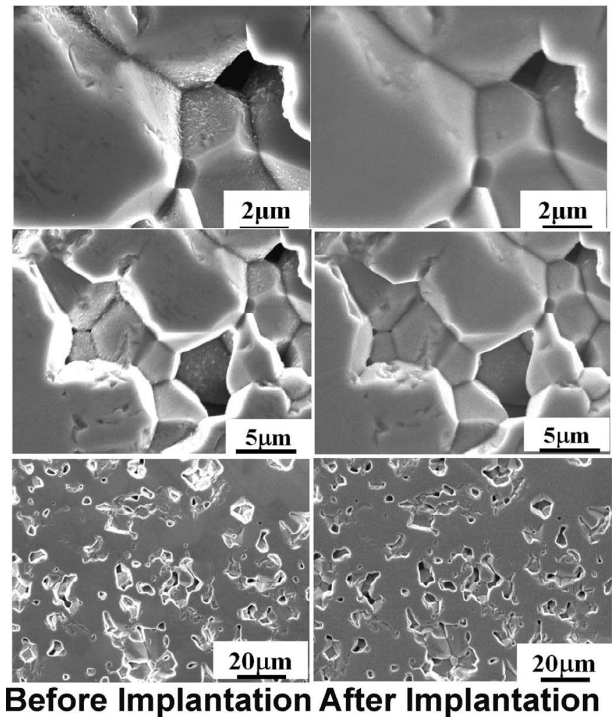

Fig. 4. Result of SEM observation of hematite surface before and after implantation (Imp-2).

before and after implantation. The change in the surface morphology was not significant, macroscopically.

Figure 4 shows an SEM image of the surface of Imp-2 before and after implantation. When the amount of implanted carbon ion became five times larger than that of Imp-1, the change in the surface morphology before and after implantation was not so clear, macroscopically. However, upon further examination, after implantation, the surface

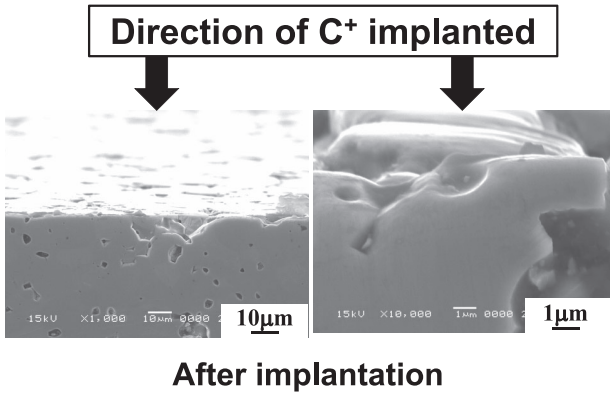

Fig. 5. SEM image of cross section of hematite (Imp-1).

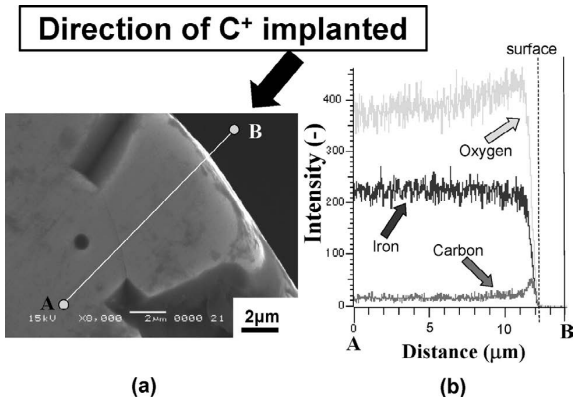

Fig. 6. Results of EDS analysis on the cross section of hematite (Imp-1). (a) SEM image (b) line analysis from the point A to B.

appeared to become rather smooth and clear, such that unstable defects and/or steps may have become stable by the collision energy of the implanted carbon. Furthermore, the electron charge on the surface may have been relieved by the modification of the electron conductivity due to the implanted carbon.

Figures 5(a) and 5(b) are cross-sectional images of Imp-1. The direction of implantation is indicated by the thick arrow in Fig. 5. From these images, it can be observed that there is little change in the structure of hematite, macroscopically, which agrees with the observations of the surface (Figs. 3 and 4). It is understood that the effect of carbon implantation is limited to a depth of around 1 μm from the surface as mentioned below.

Although the change in structure at the macroscopic level by carbon implantation was hardly observed, the elemental (Fe, O and C) distributions from the surface to the bulk and the respective binding states were examined.

3.2. EDS Analysis from the Surface to the Inside along the Cross-section

Figure 6 shows the result of line analysis of the EDS and an SEM image of the cross-section of Imp-1. The position of the line analysis is on the line AB shown in Fig. 6(a) and the distributions of Fe, O, and C are shown in Fig. 6(b). It was found that the distribution of carbon experienced a peak within 1 μm of the surface. However, the relationship between the cross-sectional area and the surface, which

must be perpendicular to the cross-sectional area, is not perfectly perpendicular and is slightly inclined. Therefore, the distribution of Fe and O was not constant near the surface (edge of cross-section), given that the distribution of carbon is clearly different from that of Fe and O. From these considerations, a simulation calculation was performed to determine the distribution of implanted carbon atoms using the program code, SRIM2003,[6] which is widely used for the analysis of implantation experiments. **Figure 7** shows the comparison of the simulation result with the experimental result shown in Fig. 6(b). In Fig. 7(a), the calculation result shows that the carbon peak position is located 0.5 μm from the surface, and the overall distribution extends to 0.75 μm. On the other hand, in Fig. 7(b), the carbon distribution extends down to 1 μm from the surface, and the peak position is located around 0.5 μm, which are in excellent agreement with the calculation when the experimental error is taken into account. It was concluded that the simulation program SRIM2003 can calculate the behavior of carbon implanted in hematite, and that the effect of the associated chemical reactions, which are not taken into account by the calculation, is negligible just after the implantation.

3.3. Theoretical Degree of Reduction with Implanted Carbon during Heating Up Experiment

In the latter part of this experiment, the heating up experiment under an argon atmosphere was carried out on samples Imp-1 and Imp-2. The reaction between the implanted carbon and hematite can be expressed as described in Eq. (1).

$$\frac{1}{3}Fe_2O_3 + C \rightarrow \frac{2}{3}Fe + CO \quad \text{..... (1)}$$

If reaction (1) occurs with 100% of the implanted carbon, the degree of reduction near the surface region can be evaluated. For a hematite surface area of 2.011 cm^2, the amounts of carbon implanted were 1.0×10^{17} ions/cm^2 for Imp-1 and 5.0×10^{17} ions/cm^2 for Imp-2, respectively. The moles of carbon were then calculated as follows.

$$\text{Imp-1: } \frac{1.0\times10^{17}\times2.011}{6.02\times10^{23}} = 3.34\times10^{-7} \text{ mol-C}$$

$$\text{Imp-2: } \frac{5.0\times10^{17}\times2.011}{6.02\times10^{23}} = 1.67\times10^{-6} \text{ mol-C}$$

In addition, although the theoretical density of hematite is 5.2 g/cm^3, the actual density of hematite used in this study was ρ_{ac}=4.8 g/cm^3, which was estimated based on the volume of the pellet (0.784 cm^3) and its weight (3.7412 g). However, as the effective depth to which the carbon was implanted could not be known, two level depths were assumed for Imp-1 and Imp-2, respectively. The depths for Imp-1 were 0.5 μm and 1 μm, and those for Imp-2 were 2 μm and 3 μm, respectively. It was assumed that all of the carbon had completely reacted with hematite in the respective volume. In this case, the moles of hematite in each effective volume were assumed to be as follows:

$$0.5\ \mu\text{m: } \frac{4.8\times1.0\times10^{-4}}{159.694} = 3.022\times10^{-6} \text{ mol-Fe}_2\text{O}_3$$

$$1\ \mu\text{m: } \frac{4.8\times2.011\times10^{-4}}{159.694} = 6.044\times10^{-6} \text{ mol-Fe}_2\text{O}_3$$

$$2\ \mu\text{m: } \frac{4.8\times4.022\times10^{-4}}{159.694} = 1.209\times10^{-5} \text{ mol-Fe}_2\text{O}_3$$

$$3\ \mu\text{m: } \frac{4.8\times6.033\times10^{-4}}{159.694} = 1.813\times10^{-5} \text{ mol-Fe}_2\text{O}_3$$

Based on Eq. (1), the degrees of reduction were estimated by assuming that all of the carbon reacted with the oxygen in hematite.

$$\text{Imp-1(0.5 } \mu\text{m): } \frac{3.34\times10^{-7}}{3.022\times10^{-6}\div3}\times100 = 33\%$$

$$\text{Imp-1(1 } \mu\text{m): } \frac{3.34\times10^{-7}}{6.044\times10^{-6}\div3}\times100 = 16.6\%$$

$$\text{Imp-2(2 } \mu\text{m): } \frac{1.67\times10^{-6}}{1.209\times10^{-5}\div3}\times100 = 41.4\%$$

$$\text{Imp-2(3 } \mu\text{m): } \frac{1.67\times10^{-6}}{1.813\times10^{-5}\div3}\times100 = 27.6\%$$

As the theoretical reduction degrees of hematite for (i) $Fe_2O_3 \rightarrow Fe_3O_4$, and (ii) $Fe_3O_4 \rightarrow FeO$ are 11% and 33%, respectively, it is understood that the reduction stage may proceed to the magnetite reduction stage ((ii) $Fe_3O_4 \rightarrow FeO$) when the reacted area is limited around the implanted surface.

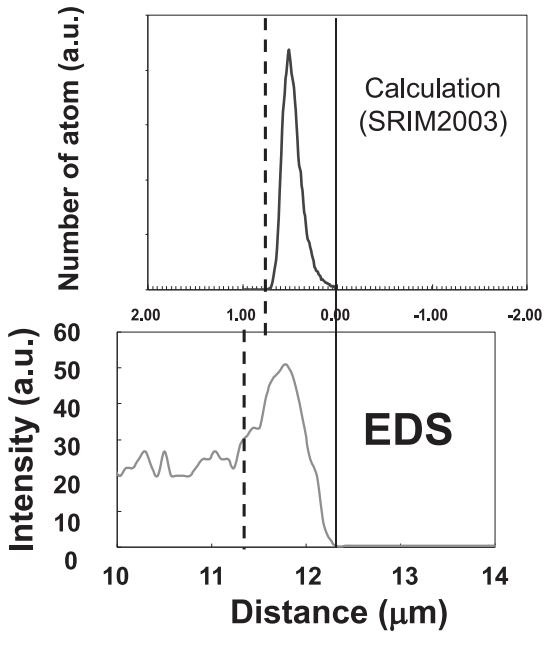

Fig. 7. Comparison of the implanted carbon distribution in hematite between experiment and calculation (SRIM2003).

3.4. XPS Measurement

3.4.1. Correction of Peak Positions of $Fe_{2p1/2}$ and $Fe_{2p3/2}$ in Hematite

The peak position measured by XPS is sometimes shifted by the effect of electron charge in the case of an insulating

material such as hematite ($\mathbf{Fe_2O_3}$). Although a charge neutralizer was used to avoid the peak shift, it is difficult to obtain the adequate neutralization point. Finally, the results were adjusted by the data reported by Grosvenor, *et al.*.[7] After these operations, the peak position for $Fe_{2p3/2}$ was determined to be 710 eV, and that for $Fe_{2p1/2}$ was determined to be 723 eV, as shown in **Fig. 8**.

In addition, Fig. 8 shows the results for metallic iron (Fe) in comparison with the reference data (JEOL, JPC-9010MC standard data book) for metallic Fe. The measurements of metallic Fe in this experiment were carried out together with argon sputtering. The surface of metallic Fe showed the effects of oxidation, while the values obtained in the bulk of metallic Fe were in excellent agreement with the reference data ($\mathbf{Fe_{2p3/2}}$ (704 eV), $\mathbf{Fe_{2p1/2}}$ (717 eV): Fig. 8 Reference). However, the peak positions of $\mathbf{Fe_{2p3/2}}$ and $\mathbf{Fe_{2p1/2}}$ in hematite were about 6 eV higher than those in metallic Fe, while those at the oxidized surface in metallic Fe were about 3 eV higher than those in metallic Fe.

The peak values for O_{1s} and C_{1s} were also corrected using the corrected values of $\mathbf{Fe_{2p3/2}}$ and $\mathbf{Fe_{2p1/2}}$, and we adopted the values when they agreed with the reference data[7] within the range of error.

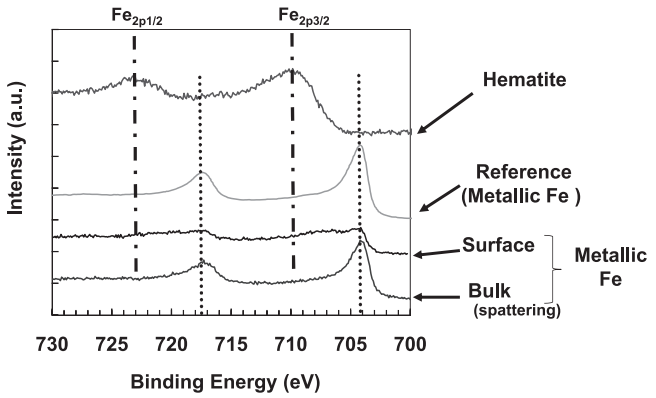

Fig. 8. Comparison of peak profiles of $Fe_{2p1/2}$ and $Fe_{2p3/2}$ in Hematite and Metallic iron.

3.4.2. Variation of Peak Profiles of $Fe_{2p1/2}$ and $Fe_{2p3/2}$ for Each Sample

Figure 9 shows the variation of the peak profiles of $\mathbf{Fe_{2p1/2}}$ and $\mathbf{Fe_{2p3/2}}$ for the samples used in this study. Figures 9(a)–9(d) correspond to the hematite sample, the hematite with a carbon layer, Imp-1 and Imp-2, respectively. The bottom profile (Ref.) in Fig. 9 represents the reference data of hematite. The second to the fourth profiles in each figure were measured by means of argon sputtering. The depth obtained by sputtering was different among the samples because the sputtering rate depended on the nature of each sample. The depths corresponding to the fourth profile in Figs. 9(a)–9(d) were 0.19 μm, 4.67 μm, 3.45 μm and 3.45 μm, respectively.

For the sputtering results, the intensities of the profiles changed toward the direction indicated by the arrows. The intensities of $\mathbf{Fe_{2p1/2}}$ and $\mathbf{Fe_{2p3/2}}$ on the surface of the samples were not detected; however, the intensities increased with sputtering time. It is obvious that the hematite with a carbon layer is completely covered with carbon; on the other hand, the other three samples (Hematite, Imp-1 and Imp-2) experienced relatively strong effects of carbon contamination on their surfaces.

3.4.3. Variation of Peak Profiles of O_{1s} for Each Sample

Figure 10 shows the variation of the peak profiles of $\mathbf{O_{1s}}$. The profiles were obtained in the same way as mentioned above. The intensities of $\mathbf{O_{1s}}$ increased with the depth from the surface, and the direction of the changes are indicated by the arrows in Fig. 10. Basically, the directions of the changes were the same among Figs. 10(a)–10(c), while the intensity of $\mathbf{O_{1s}}$ of Imp-2 decreased and then increased as shown in Fig. 10(d). This result was caused by the relative concentration of carbon. As mentioned above, the carbon distribution of Imp-1 extended down to 1 μm from the surface, and the maximum value was located at 0.5 μm. As the amount of carbon implanted in Imp-2 was 5 times larger than that in Imp-1, the carbon would have distributed deeper into Imp-2. For this reason, the intensities of carbon concentration (the details will be mentioned in the next section)

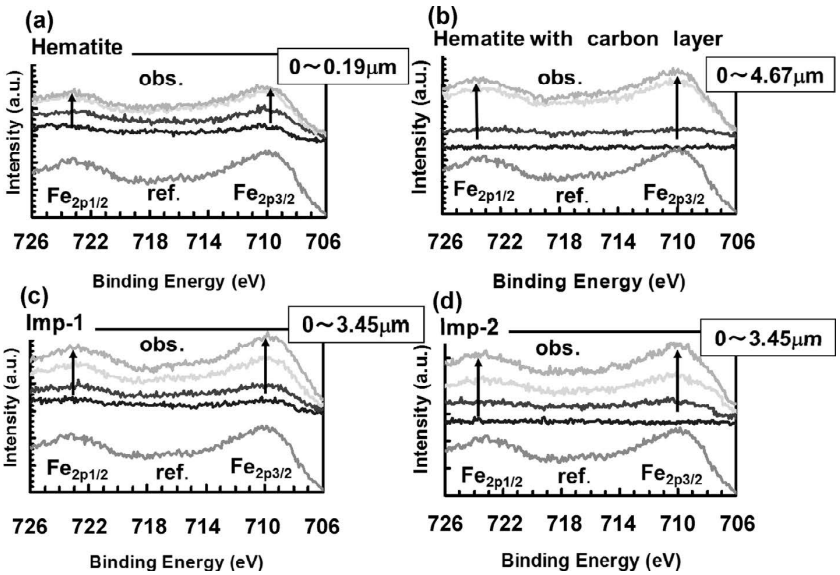

Fig. 9. Variation of peak profiles of $Fe_{2p1/2}$ and $Fe_{2p3/2}$ peaks.

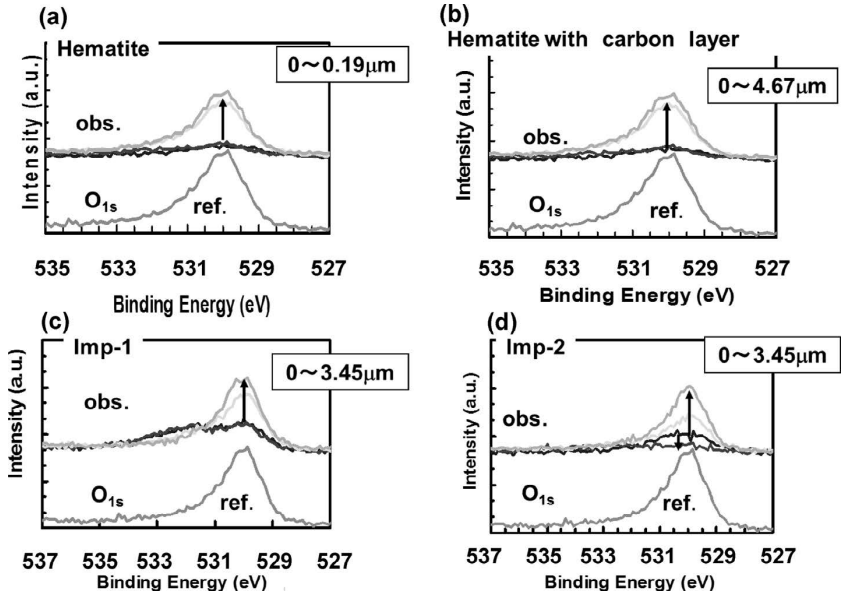

Fig. 10. Variation of peak profiles of O_{1s}.

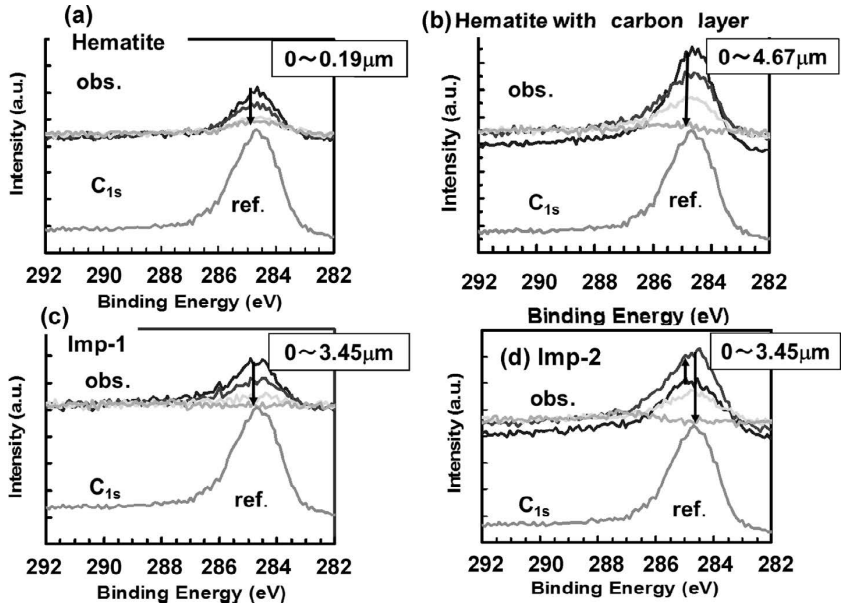

Fig. 11. Variation of peak profiles of C_{1s}.

increased and then decreased. To the contrary, oxygen distribution once decreased and then increased. In addition, as the sputtering depth for one measurement was relatively large in this experiment, the variation in the carbon concentration for Imp-1 experienced a monotonous increase. If the sputtering depth had been shallower, the variation in carbon concentration of Imp-1 would have also shown the same tendency as Imp-2.

3.4.4. Variation of Peak Profiles of C_{1s} for Each Sample

Figure 11 shows the variation of the peak profiles of C_{1s} for the samples used in this study, and the arrows indicate the directions of the change of the main peaks with argon sputtering. The hematite sample shows a carbon peak caused by contamination and a carbon intensity that decreases from the surface to the bulk. Beyond a depth of 0.19 μm, the carbon intensity is almost negligible.

As mentioned above, the intensity of C_{1s} changed in a manner opposite to the intensity of O_{1s} (Figs. 10 and 11). The intensity of C_{1s} of Imp-2 increased and then decreased, which corresponds to the carbon distribution in the hematite sample created by implantation.

Figure 12 shows the variation of the maximum intensity of C_{1s} as a function of the depth from the surface. The results for graphite are also plotted in Fig. 12 for the sake of comparison. The carbon layer on the hematite surface was extremely thin, less than about 0.19 μm, which might have been contaminated inside the SEM and in the ambient atmosphere. The depths corresponding to 80% of the maximum intensity of C_{1s} were about 0.7 μm and 2.0 μm for Imp-1 and Imp-2, respectively. However, the results for Imp-1 were rather different from the results of the EDS analysis and the simulation calculation shown in Fig. 7. This cause might have been due to the effects of carbon contam-

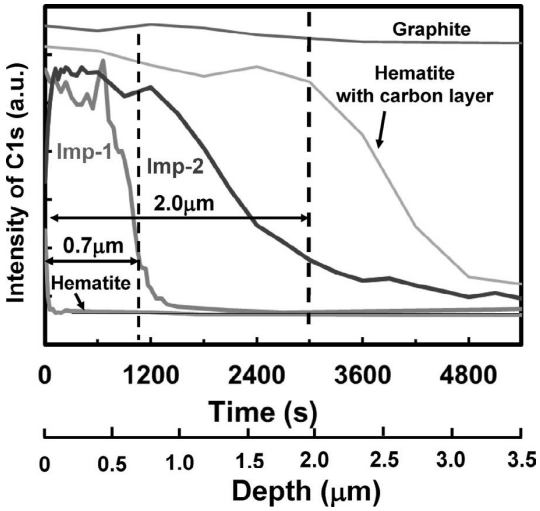

Fig. 12. Variation of the maximum value of C_{1s} peaks.

ination on the surface and argon sputtering, which induced the diffusion of carbon. In the case of Imp-2, the carbon distribution was detected at a deeper position than 3.5 μm with statistical significance, which meant that a relatively high rate of diffusion of carbon occurred even in an iron oxide.

The hematite with a carbon layer showed a high constant carbon concentration until 2 μm from surface, from where the value decreased moderately in the range from 2 μm to 3 μm. The thickness of the carbon layer deposited was estimated to be 300 nm in other experiments.[5] This difference might be caused by the following: (1) a different sputtering rate between the carbon layer and hematite, (2) significant carbon diffusion into the hematite structure during sputtering. Because the distances along the horizontal axis are not absolute values for the different materials, a more precise experiment should be conducted in the future. The results for graphite are plotted for comparison and show the highest intensities, while the deposited carbon layer on the hematite showed lower intensities than those of graphite; these differences correspond to the difference in carbon density.

3.4.5. Peak Separation of C_{1S} and the Different Kinds of Binding Modes of Carbon

Figure 13 shows an example of the peak separation in the profile of C_{1s}. The binding energies of C=O, C–O, C–C and C–Fe were determined to be 287.3 eV, 285.7 eV, 284.3 eV and 283.1 eV, respectively. The changes in the peak position in each measurement were within ±0.3 eV. The present values of the peak positions are 0.5 eV to 0.9 eV higher than those obtained by Estrade-Szwarckopf[8] and Plyuto *et al.*.[9]

The intensities at the separated binding energies are plotted against the depth from the surface for Imp-2, as shown in **Fig. 14**. The C–C bond has the highest intensity, the value of which corresponds to the axis on the left-hand side of the graph. The intensities for C–O, C=O and C–Fe bonds correspond to the axis located at the right-hand side of the graph. The C–C bond shows a high value until 0.5 μm from the surface, beyond which the intensity decreases monotonously. On the other hand, the C–O bond shows a larger intensity than the C=O bond and shows almost twice the intensity until 1 μm from the surface; moreover, it reaches almost the same value from 1 μm, and it is understood that

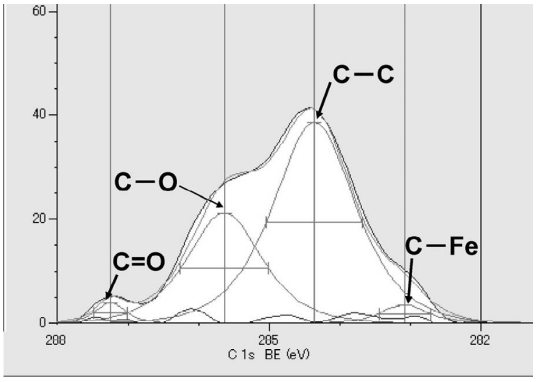

Fig. 13. Example of a peak separation of C_{1s} peak.

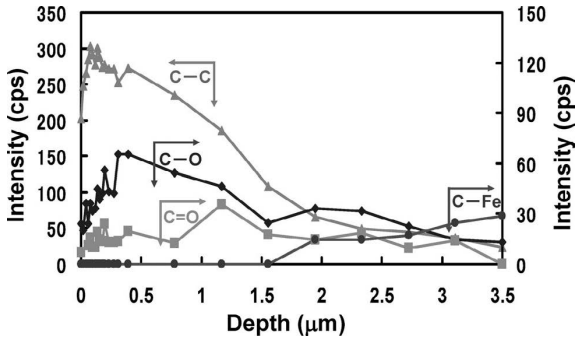

Fig. 14. Variation of intensities for the C–C, C–O, C=O and C–Fe bond in C_{1S} as a function of the depth from surface (Imp-2).

the C–O and C=O bonds correspond to the reduction products, CO or CO_2 gases, which are generated during the heating reduction.

The intensity of the C–Fe bond becomes significant beyond 1.5 μm. It is assumed that this kind of bond might be close to the state of iron carbide; however, the C–Fe bond will transform to a C–O and/or C=O bond when the reduction reaction proceeds and the reaction interface is moved because the iron carbide state is not thermodynamically stable.

3.5. Heating Up Reduction under an Inert Atmosphere

3.5.1. *In situ* Observation by Laser Microscope

Figure 15 shows the results of *in situ* observations of the reaction behavior of Imp-1 during the heating up experiment using a laser microscope under an argon atmosphere. The heating up conditions were as follows: 3 min to 1 000°C (5.56 K/s), held at 1 000°C for 30 min and quenched to the ambient temperature in 3 min. Figure 15 shows still images captured from a movie recorded on a DVD. Although the temperature was 360°C in the sample shown in Fig. 15(a), the surface appears the same as it did before the reaction. Figures 15(b)–15(e) show the sample surface during reaction in the course of being heated to temperatures of 463°C, 635°C, 1 030°C and 1 031°C, respectively. Figure 15(f) is the image of the final stage of the reaction. There was no change in the sample from the final stage shown in Fig. 15(f) to room temperature. From these photos, the reaction behaviors of Imp-1 appear to be quite complex, and the morphology of the surface changes significantly during reaction.

Because it is difficult to analyze such images, the follow-

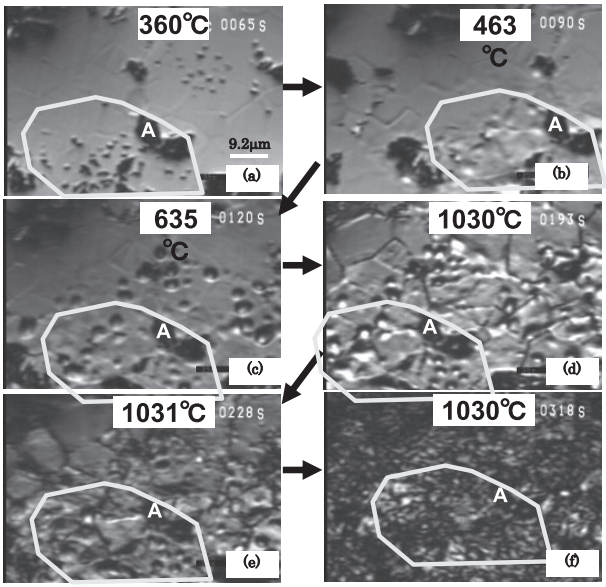

Fig. 15. *In situ* observation of the heating up experiment under argon atmosphere by laser microscope (Imp-1).

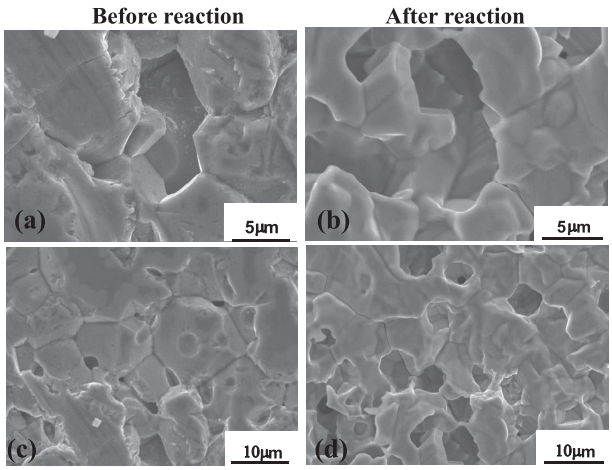

Fig. 16. Microstructure of the surface of Imp-1 before and after heating up experiment.

ing procedures were adopted. The character 'A' in Fig. 15 indicates a relatively large pore. The marked pore did not change significantly during the experiment. The structure near 'A', which is outlined by a white solid line, was mainly analyzed during the experiment. In addition, the structure marked 'A' was not set to one position in the monitor because the pedestal that the crucible was set on was moved by the expansion during heating so that the marked position 'A' was manually adjusted to come to one point during the experiment. As a result, the positions of 'A' vary slightly among Figs. 15(a)–15(f).

Figure 15(b) shows the beginning of the reaction at a temperature of 463°C. The small pores and/or apophyses (<1 μm) around 'A' disappeared simultaneously in a moment, and many shallow dimples were formed at the region marked 'A' up to 635°C just before the state shown in Fig. 15(c). At 635°C, as shown in Fig. 15(c), round clear dimples were formed around the region marked 'A'. As the temperature increased, the number of dimples (Figs. 15(d), 15(e)) increased, and dynamic movement of the surface was observed in the movie. Finally, as shown in Fig. 15(f), a complex heteroclite structure less than 1 μm in size was formed.

3.5.2. SEM Observation of the Surface before and after Reaction

Figure 16 shows an SEM image of the surface of Imp-1 before and after heating. Figures 16(a) and 16(c) show the surface before heating. Even before heating, there are many holes and grain boundaries similar to those shown in Fig. 3 and Fig. 4. However, after the heating experiment, further intense convex-concave structures were generated, and a very different surface structure appeared.

Figures 16(a) and 16(b) compare the surface structure at the same position before and after heating at relatively large magnification. Each grain significantly contracted, and many holes at the grain boundary were generated. The original shape of the grain was hardly maintained after heating. Figures 16(c) and 16(d) are lower-magnification images before and after heating. Large pores about 5 μm in diameter were generated and increased in number in the vicinity of the grain boundaries. The development of complex surface morphology after heating was caused by these holes. The overall reaction is describe by Eq. (2).

$$Fe_xO_y + C = Fe_xO_{y-1} + CO \quad \text{..... (2)}$$

Carbon is the implanted species and reaction (2) occurs inside the hematite structure. The evolved CO gas should diffuse to the outside of hematite through the grain boundaries. The reaction might then occur in the vicinity of the grain boundaries. On the other hand, a trapped gas may be pressurized, and the surface of hematite will be lifted up and produce dimples when the pressure is released. Such dynamic movement was actually observed as mentioned above.

It seemed that the reaction between hematite and the implanted carbon proceeded in two stages; one at about 450°C and the other at 630°C. The former reaction around 450°C might correspond to a rearrangement of the hematite structure, although a small extent of reaction between carbon and hematite might exist. The reaction around 630°C is a reduction reaction expressed as by Eq. (2), during which gas evolution and dynamic movement occur. Unfortunately, because there is currently no concrete evidence for these assumptions, more precise gas analyses near the surface should be performed in the near future.

The reaction between hematite and the carbon layer deposited on the hematite was reported in a previous study.[5] The beginning of the reduction reaction occurs from 646 to 650°C, which is close to the temperature at which the second stage of the reaction between hematite and implanted carbon occurs. It is concluded that the reaction itself is the same between hematite and carbon; however, the behavior must vary with the location between carbon and hematite. In particular, it could be an important factor in understanding how the evolved CO gas escapes the reaction site.

3.5.3. Reaction Mechanism

Figure 17 shows the mechanism between the carbon layer and hematite.[5] When the carbon layer becomes thicker than 300 nm, the evolved CO gas cannot be liberated to the

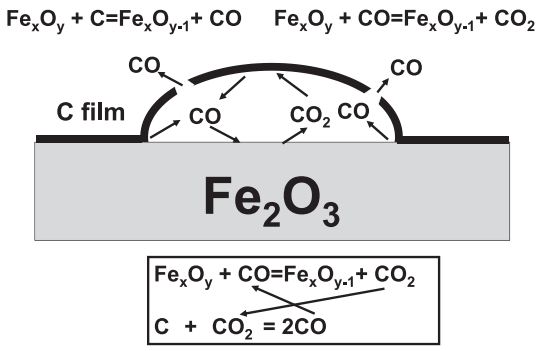

Fig. 17. Illustration of the mechanism of reaction between Fe_2O_3 and carbon film.[5)]

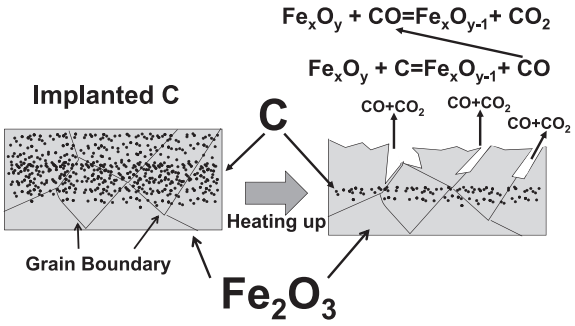

Fig. 18. Illustration of the mechanism of reaction of Fe_2O_3 and carbon implanted.

outside, and swelling of the carbon film occurs. The reaction for the generation of CO_2 can be expressed by Eq. (3).

$$Fe_xO_y + CO = Fe_xO_{y-1} + CO_2 \quad \text{..... (3)}$$

When reaction (3) occurs, the Boudouard reaction (4) between the carbon film and CO_2 will occur.

$$CO_2 + C = 2CO \quad \text{..... (4)}$$

Until a part of the carbon film is consumed by the reaction (4) and the gases are liberated to the outside, reactions (2) and (3) will proceed simultaneously, and thermodynamic coupling will occur.[10,11)]

On the other hand, the reaction between the implanted carbon and hematite is also initiated by reaction (2), and the mechanism for it is shown in **Fig. 18**. However, as the reaction occurs in the hematite structure, the evolved gas CO cannot go outside easily. The gas will be pressurized around the reaction site, and swelling of hematite may occur. In the next stage, when the gas is liberated, a dimple will form, and sometimes, a large hole will be generated. These sequences are in agreement with the *in situ* observations mentioned above. The CO_2 concentration might be high when the storage time of CO gas inside the hematite is long because reaction (3) occurs dominantly. In this study, it is assumed that reaction (3) for the generation of CO_2 occurs to some extent. The reaction mechanism is summarized in Fig. 18 in which the surface roughness generated by reactions (2) and (3) occurs along the grain boundary.

4. Conclusions

Hematite with carbon implantation was observed using SEM and EDS. The binding energies of Fe, C and O were measured by XPS. Furthermore, the carbon-implanted hematite was heating up under an argon atmosphere, and the reaction behaviors were observed *in situ*. The results obtained are as follows:

(1) A macroscopic change in surface structure was not observed before and after implantation.

(2) The distribution of implanted carbon extended to 1 μm below the surface of Imp-1 and 2 μm below the surface of Imp-2.

(3) The distribution of implanted carbon was in agreement with the results obtained by SIRIM2003.

(4) In the heating up experiment, under an argon atmosphere, the reactions between implanted carbon and hematite proceeded in two stages at 450°C and 630°C. The reaction that occurred at 450°C is a rearrangement of the hematite structure distorted by the implanted carbon. The one at 630°C is the direct reaction between the carbon and hematite.

(5) With respect to the reaction between hematite and the carbon, the starting temperature of the reaction is almost the same from 630°C to 650°C. However, the reaction behavior varied with the location of carbon and hematite.

Acknowledgement

A part of this study was conducted with the support of the "ISIJ Research Promotion Grant in 2008" and also the "Grant-in-Aid for Scientific Research B (21310061)" from the Ministry of Education, Culture, Sport, Science and Technology in Japan.

REFERENCES

1) J. Vahdati Khaki, Y. Kashiwaya, Y. Suzuki and K. Ishii: *ISIJ Int.*, **42** (2002), 13.
2) Y. Kashiwaya, H. Suzuki and K. Ishii: *ISIJ Int.*, **44** (2004), 1970.
3) Y. Kashiwaya, H. Suzuki and K. Ishii: *ISIJ Int.*, **44** (2004), 1975.
4) Y. Kashiwaya and K. Ishii: *ISIJ Int.*, **44** (2004), 1981.
5) Y. Kashiwaya, Y. Yamaguchi, H. Kinoshita and K. Ishii: *ISIJ Int.*, **47** (2007), 226.
6) J. F. Ziegler, J. P. Biersack and U. Littmark: SRIM, The Stopping and Range of Ions in Solids, Pergamon Press, New York, (1985) (new edition in 2009).
7) A. P. Grosvenor, B. A. Kobe, M. C. Biesinger and N. S. Mclntyre: *Surf. interface anal.*, **36** (2004), 1564.
8) H. Estrade-Szwarckopf: *Carbon*, **42** (2004), 1713.
9) I. V. Plyuto, A. P. Shpak, J. Stoch, L. F. Sharanda, Y. V. Plyuto, I. V. Babich, M. Makkee and J. A. Moulijn: *Surf. interface anal.*, **38** (2006), 917.
10) Y. Kashiwaya, M. Kanbe and K. Ishii: *ISIJ Int.*, **41** (2001), 818.
11) Y. Kashiwaya, M. Kanbe and K. Ishii: *ISIJ Int.*, **46** (2006), 1610.